Power Electronic Systems
Laboratory

IEEE Transactions on Energy Conversion, Vol. 28, No. 3, pp. 493-501, September 2013

Split Ratio Optimization for High-Torque PM Motors Considering Global and Local Thermal Limitations

T. Reichert,
T. Nussbaumer,
J. W. Kolar

Eidgenössische Technische Hochschule Zürich
Swiss Federal Institute of Technology Zurich

Split Ratio Optimization for High-Torque PM Motors Considering Global and Local Thermal Limitations

Thomas Reichert, *Member, IEEE*, Thomas Nussbaumer, *Member, IEEE*, and Johann W. Kolar, *Fellow, IEEE*

***Abstract*—The split ratio of an interior rotor permanent-magnet machine, which relates the rotor diameter to the total motor diameter, can be optimized with the goal of generating maximum torque for a given motor volume. For that purpose, thermal constraints have to be considered that limit the producible magnetomotive force and, consequently, the torque output. Both a maximum local current density in the coils and a maximum global copper loss density related to the motor surface are respected. In this paper, the analytical calculations for torque and split ratio are derived and the influence of these thermal constraints is elaborated.**

***Index Terms*—Brushless motors, design optimization, permanent-magnet motors, temperature, torque.**

I. Introduction

PERMANENT-MAGNET machines are employed in a wide range of applications such as pumps, mixers, and stirrers, pervading numerous industrial sectors [1]–[5]. They generally consist of a slotted stator with copper windings and an interior rotor built of permanent magnets and iron. For a large percentage of these industrial applications, the motor design aims at maximizing the torque while respecting two important boundary conditions. To begin with, the outer motor dimensions are usually fixed as they result from the application itself. The second important constraint is given by physical limitations, namely, thermal limitations and magnetic saturation in the iron parts of the motor [6]–[9]. Obviously, these physical limitations can be influenced by the choice of the motor materials, yet there is usually a threshold for each application where the improvement of material properties is outweighed by the rising material costs. Hence, for fixed boundary conditions, the motor torque has to be maximized by means of varying the dimensions of the rotor, iron and copper parts inside the machine. It was found that the ratio of rotor diameter to total motor diameter, the so called split ratio [10], is highly relevant to the torque output.

In preceding publications, the split ratio has been optimized under the constraint of fixed copper losses [11]–[13]. At first sight, this constraint seems meaningful since the outer dimensions of the machine stay constant and a certain constant amount of heat can be dissipated via the motor surface. However, this assumption does not consider local thermal situations inside the motor, especially for the stator coils, which are the main heat source during an operation under full load. For an increasing split ratio, the stator area and, consequently, the winding space get reduced. Hence, a local thermal limitation in the copper windings has to be considered additionally, which can be accounted for with a limited current density, as will be further elaborated in this paper.

This paper expands the current findings about the optimal split ratio for permanent-magnet machines with nonoverlapping (concentrated) windings. The focus lies on high-torque machines that run at low to moderate rotational speeds. In Section II, the existing analytical torque calculation is summarized and expanded with the influence of the local thermal limitation in the coils. In Section III, the optimal split ratio calculation is derived respecting both thermal constraints. Three cases can be distinguished, with either one of the thermal constraints being the decisive factor for the optimal split ratio or, as the third option, with both constraints determining the optimal split ratio. The distinction between these three cases depends on the actual values of the thermal limitations and the motor dimensions, as will be shown in Section IV. The identification of the actual thermal values and their interconnection is addressed in Section V, and finally, in Section VI, the findings from this analysis are transformed into general design guidelines for this machine type.

II. Torque Calculation

The torque calculation for a radial-flux machine is based on the (tangential) Lorentz force. For one concentrated coil, the maximum force is given by

$$F_{\mathrm{coil,max}} = \underbrace{(N_{\mathrm{coil}} \cdot \hat{I})}_{\hat{\Theta}} \cdot 2l \cdot B \tag{1}$$

with the peak magnetomotive force $\hat{\Theta}$, which is the product of the coil winding number N_{coil} and the peak winding current $\hat{I}$, the active motor length (or height, respectively) l, and the air gap flux density B. The last multiplication in (1) is allowed because of the perpendicular arrangement of axial current, radial flux, and tangential force. The factor $2l$ in (1) is due to the fact that each conductor of a coil passes the air gap twice, but at different positions with opposing permanent-magnet flux density direction.

The constant torque value T of any m-phase machine running in sinusoidal mode is found by multiplying the Lorentz force F

Manuscript received June 18, 2012; revised March 1, 2013; accepted April 14, 2013. Date of publication May 20, 2013; date of current version August 16, 2013. Paper no. TEC-00278-2012.

T. Reichert and J. W. Kolar are with the Power Electronic Systems Laboratory, ETH Zurich, 8092 Zurich, Switzerland (e-mail: reichert@lem.ee.ethz.ch; kolar@lem.ee.ethz.ch).

T. Nussbaumer is with the Levitronix GmbH, 8005 Zurich, Switzerland (e-mail: nussbaumer@levitronix.com).

Color versions of one or more of the figures in this paper are available online at http://ieeexplore.ieee.org.

Digital Object Identifier 10.1109/TEC.2013.2259169

with the air gap radius r, resulting in

$$T = \frac{Q}{m} \cdot \frac{m}{2} \cdot F_{\mathrm{coil,max}} \cdot r = Q \cdot N_{\mathrm{coil}} \cdot \hat{I} \cdot l \cdot B \cdot r \quad (2)$$

where Q is the slot number, which, in the case of concentrated windings, equals the number of coils. The slot to phase ratio Q/m has to be considered as well as a factor $m/2$, which links the maximum force of one coil with the resulting constant torque for an m-phase system in sinusoidal mode.

In order to achieve the highest possible torque, the magnetomotive force has to be maximized. This maximum reachable value is determined by the thermal limitations of the motor, which can be split into two categories. There is a global thermal limitation, which is defined by the allowed total motor losses related to the motor surface. For the targeted high-torque machines with moderate rotational speeds, the iron losses can be kept in a reasonable range if the iron parts are well designed (e.g., thin lamination). Hence, the dominating motor losses are the ohmic copper losses. The second thermal constraint is local, concerning the coils. The current density in the coil windings has to be limited in order to avoid local overheating, which would lead to the destruction of the winding insulation and result in a short circuit.

A. Torque with Global Thermal Limitation

According to Pang *et al.* [11], the optimal split ratio is slightly lowered when the end-windings are considered for the copper loss calculation. However, as this influence on the final result is typically quite small, the end-windings will be neglected in the further analysis for means of simplicity and clarity. Nevertheless, for specific machine designs such as pancake geometry, the end-windings become influential and would have to be considered. This influence could be modelled with an equivalent motor length l_e [11], which would have to be used instead of the active motor length l in the following. With this measure, the analysis could be conducted in the same way just with a different dimension for the motor length.

The total copper losses P_{Cu} can be described as

$$P_{\mathrm{Cu}} = Q \cdot I_{\mathrm{rms}}^2 \cdot \rho_{\mathrm{Cu}} \cdot \frac{N_{\mathrm{coil}} \cdot 2l}{A_{\mathrm{wdg}}} \quad (3)$$

where ρ_{Cu} is the resistivity of copper. The area of one single copper winding A_{wdg} is given by

$$A_{\mathrm{wdg}} = \frac{A_{\mathrm{coil}} \cdot k_{\mathrm{coil}}}{N_{\mathrm{coil}}} \quad (4)$$

depending on the available cross-sectional area A_{coil} of one concentrated coil and the slot fill factor k_{coil}. Then, the total copper losses can be reformulated to

$$P_{\mathrm{Cu}} = Q \cdot \frac{\hat{I}^2}{2} \cdot \rho_{\mathrm{Cu}} \cdot \frac{N_{\mathrm{coil}}^2 \cdot 2l}{A_{\mathrm{coil}} \cdot k_{\mathrm{coil}}}. \quad (5)$$

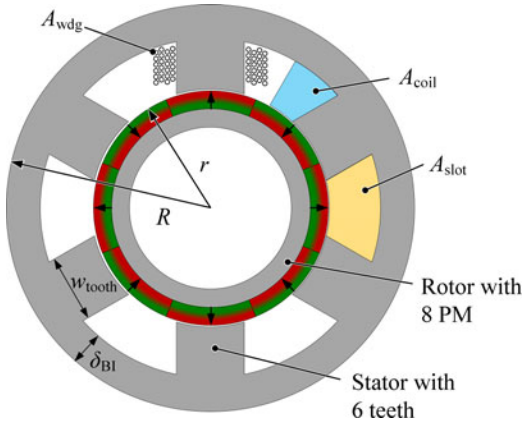

Fig. 1. Schematic drawing of an interior rotor motor. This exemplary topology consists of a stator with six stator teeth and a rotor with eight permanent magnets and a back iron ring. The permanent magnets are diametrically magnetized in alternating order.

For the maximum allowed copper losses $P_{\mathrm{Cu,max}}$, (5) can be rearranged to solve for $\hat{I}$, and the resulting term is then integrated into (2), leading to a torque function of

$$T = \sqrt{\frac{P_{\mathrm{Cu,max}} \cdot A_{\mathrm{coil}} \cdot k_{\mathrm{coil}} \cdot l \cdot Q}{\rho_{\mathrm{Cu}}}} \cdot B \cdot R \cdot \chi \quad (6)$$

with R being the outer radius of the stator core and χ being the split ratio, defined as

$$\chi = \frac{r}{R}. \quad (7)$$

B. Torque with Local Thermal Limitation

Up to now, the analysis has been based on a global thermal limitation, which was respected by fixing the total copper losses. However, if the split ratio is enlarged, the coils become smaller, while the losses remain constant and, consequently, the local temperature rises. Thus, an additional local thermal limitation has to be respected, which can be done by fixing the maximum allowed current density J_{max} in the windings. Then, the current per coil is limited by

$$(N_{\mathrm{coil}} \cdot I_{\mathrm{rms}})_{\mathrm{max}} = J_{\mathrm{max}} \cdot A_{\mathrm{coil}} \cdot k_{\mathrm{coil}}. \quad (8)$$

Combining (5) and (8), the relationship between the copper losses and the current density can be determined as

$$J = \sqrt{\frac{P_{\mathrm{cu}}}{Q \cdot \rho_{\mathrm{Cu}} \cdot 2l \cdot A_{\mathrm{coil}} \cdot k_{\mathrm{coil}}}}. \quad (9)$$

The available torque can be found by combining the constraint in (8) with the formula in (2), leading to

$$T = \sqrt{2} Q \cdot J_{\mathrm{max}} \cdot A_{\mathrm{coil}} \cdot k_{\mathrm{coil}} \cdot l \cdot B \cdot R \cdot \chi. \quad (10)$$

III. Split Ratio Calculation

In order to be able to determine the optimal split ratio, the influence of this split ratio on the cross-sectional coil area has

to be established first. As shown in Fig. 1, the available cross-sectional area A_{coil} of one coil equals half the slot area A_{slot}

$$A_{\mathrm{slot}} = 2A_{\mathrm{coil}}. \tag{11}$$

Obviously, this slot area is highly influenced by the split ratio. Additionally, for this kind of split ratio analysis, the flux density ratio β, defined as

$$\beta = \frac{B}{B_{\mathrm{Fe,max}}} \tag{12}$$

is introduced [10]–[13], which relates the air gap flux density B to the maximum allowed flux density in the stator teeth $B_{\mathrm{Fe,max}}$. The stator tooth width required to avoid iron saturation and respect this maximum allowed flux density becomes

$$w_{\mathrm{tooth}} = \frac{2\pi \cdot r \cdot \beta}{Q} \tag{13}$$

whereas for the stator back iron thickness δ_{BI}, a value of half the tooth width is assumed in the case of nonoverlapping windings. These assumptions for the stator dimensions and the flux density relation according to (12) are commonly used for split ratio optimization.

The available slot area

$$A_{\mathrm{slot}} = \underbrace{\frac{\pi \cdot \left(R^2 - r^2\right)}{Q}}_{\text{Stator area/slot}} - \underbrace{\frac{\pi \cdot R^2 - \pi \cdot \left(R - \delta_{\mathrm{BI}}\right)^2}{Q}}_{\text{Back iron area/slot}} - \underbrace{w_{\mathrm{tooth}} \cdot \left(R - \delta_{\mathrm{BI}} - r\right)}_{\text{Stator tooth area}} \tag{14}$$

can be rewritten as

$$A_{\mathrm{slot}} = \frac{\pi \cdot R^2}{Q}\left(f_a \cdot \chi^2 - 2f_b \cdot \chi + 1\right) \tag{15}$$

with the two factors

$$f_a = \frac{\pi}{Q} \cdot \left(\frac{\pi}{Q} + 2\right) \cdot \beta^2 + 2\beta - 1 \tag{16}$$

and

$$f_b = \left(\frac{\pi}{Q} + 1\right) \cdot \beta. \tag{17}$$

A. *Split Ratio With Global Thermal Limitation*

As in [9], the optimal split ratio as a function of β can be found by differentiating the torque according to (6) with respect to χ, and solving the equation

$$\frac{\partial T}{\partial \chi} = 0. \tag{18}$$

In this case, the optimal split ratio χ becomes

$$\chi_P = \frac{b_P - \sqrt{b_P^2 - 4a_P}}{2a_P} \tag{19}$$

with the factors

$$a_P = 2f_a \tag{20}$$

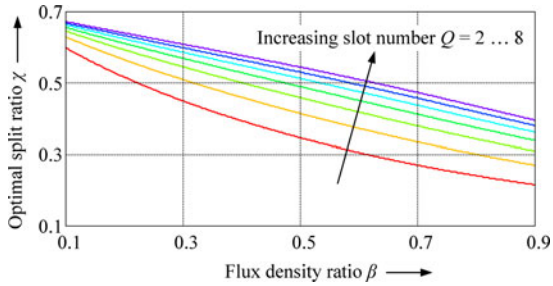

Fig. 2. Optimal split ratio according to (19), respecting a global maximum for the copper losses. It increases when the slot number is enlarged (from $Q = 2$ to 8) and decreases for a growing flux density ratio.

and

$$b_P = 3f_b. \tag{21}$$

It should be noted that the optimal split ratio only depends on two values, namely, the flux density ratio and the slot number. In Fig. 2, (19) is applied in order to show the optimal split ratio as a function of these two parameters. It can be seen that the split ratio decreases for a growing flux density ratio. This is due to the increase in the required iron area (stator back iron and stator teeth) in the case of a larger flux density. Hence, the available rotor space and the split ratio are lowered. On the other hand, the optimal split ratio is increased for motors with a larger slot number. When the number of stator teeth (equal to the slot number) is increased, each of the teeth individually becomes narrower, which leads to a decrease in back iron thickness and, consequently, allows for more space for the rotor. The remaining parameters such as the maximum allowed copper losses, the slot fill factor, or the machine radius do not influence the optimal split ratio in this case. Nevertheless, there is an important influence of these parameters for the torque calculation according to (6). Moreover, these parameters highly influence the optimal split ratio if both global and local thermal limitations are respected, as will be further elaborated later in this paper.

In the upper plot of Fig. 3(a), the torque output is shown for a motor with slot number six and three geometric dimensions, this equals about 190 W of total copper losses. Previous publications would stop their analysis at this point, which can be misleading, as will be shown in the following. The corresponding current densities in the coils according to (9) are plotted in the lower plot of Fig. 3(b). A maximum allowed current density of 10 A/mm^2 has been set, which is marked with a boundary line. It can be seen that the current density grows when increasing the split ratio. For the chosen limitations, the boundary for the current density is reached before the optimal split ratio value (maximum torque). Hence, the local thermal limitation would be violated for the optimal split ratio according to (19), which, consequently, cannot be counted as a valid design point. There is obviously interdependence between the global and local thermal limitation. Nevertheless, a motor designer can choose these parameters freely over a wide value range by modifying the thermal convection on the motor surface (e.g., employing different heat sinks), which influences the global thermal limitation itself, and the thermal conductivity inside the mixer (e.g., using different

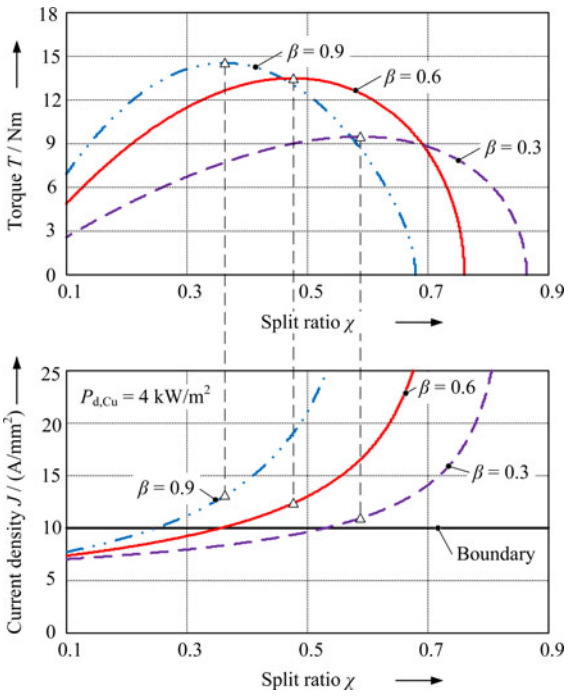

Fig. 3. Torque output for an interior rotor machine with slot number 6 is shown in the upper plot for a fixed copper loss density of 4 kW/m^2 as a function of the split ratio for three different flux density ratios. The corresponding current densities in the coils are plotted below. If a maximum current density of 10 A/mm^2 is respected, it can be seen that the maximum output torque (optimal split ratio) is actually not a valid operating point ($R = 75$ mm, $l = 25$ mm, $N_{\mathrm{coil}} = 300$, and $k_{\mathrm{coil}} = 0.6$).

pottants), which alters the relationship between the global and local thermal limitation.

B. Split Ratio With Local Thermal Limitation

As can be seen in Fig. 3, a violation of the local thermal limitation can occur if only the copper losses are addressed in the split ratio calculation. Hence, an alternative derivation according to (18) can be applied using the torque determined in (10).

In this case, the optimal split ratio becomes

$$\chi_J = \frac{b_J - \sqrt{b_J^2 - 4a_J}}{2a_J} \tag{22}$$

with different factors

$$a_J = 3f_a \tag{23}$$

and

$$b_J = 4f_b. \tag{24}$$

As described earlier, the optimal split ratio only depends on the flux density ratio β and the slot number Q. Its optimal value for different flux density ratios and slot numbers is given in Fig. 4. The characteristics are similar to those shown in Fig. 2. However, the optimal split ratio is always smaller compared to the split ratio according to (19).

In the lower plot of Fig. 5, the torque output is shown for a motor with slot number 6 and three different flux density ratios,

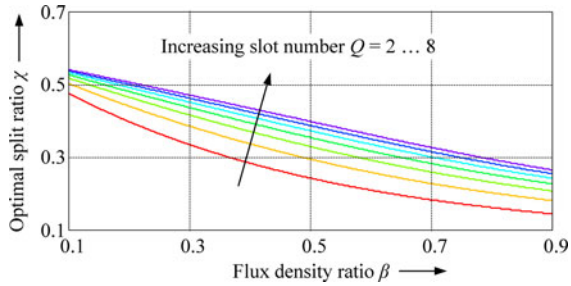

Fig. 4. Optimal split ratio according to (22), respecting a local maximum current density in the coils. It increases when the slot number is enlarged (from $Q = 2$ to 8) and decreases for a growing flux density ratio. The optimal split ratio is always smaller compared to the split ratio with the constraint of a global maximum for the copper losses (see Fig. 2).

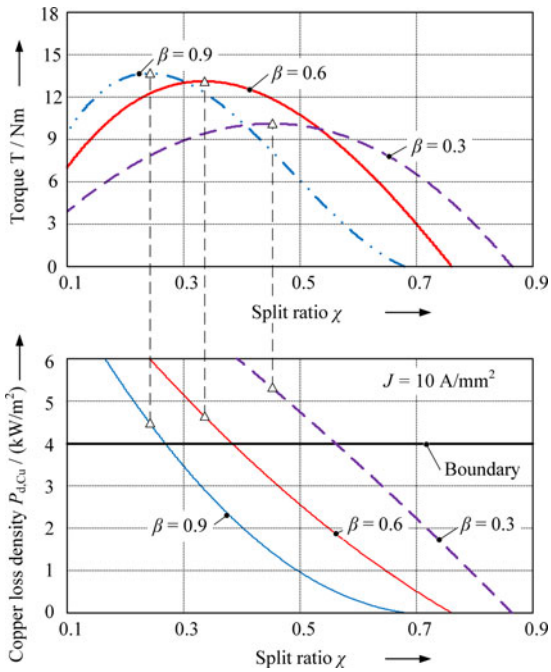

Fig. 5. Torque output for an interior rotor machine with slot number 6 is shown in the upper plot for a fixed current density of 10 A/mm^2 as a function of the split ratio for three different flux density ratios. The corresponding total copper loss density is plotted below. If a maximum of 4 kW/m^2 is respected for this loss density, it can be seen that the maximum output torque (optimal split ratio) is actually not a valid operating point ($R = 75$ mm, $l = 25$ mm, $N_{\mathrm{coil}} = 300$, and $k_{\mathrm{coil}} = 0.6$).

similar to Fig. 3. This time, however, the torque calculation according to (10) has been used with a maximum allowed current density of 10 A/mm^2. As expected, the maximum torque is achieved for smaller split ratio values than achieved earlier. The corresponding total copper loss density $P_{d,\mathrm{Cu}}$ is plotted below in Fig. 5. Additionally, the previously set maximum of 4 kW/m^2 is marked with a boundary line. It can be seen that the copper losses decrease for increasing split ratio values. In this case, the chosen limitations for the copper losses are violated for the optimal split ratio (maximum torque) according to (22).

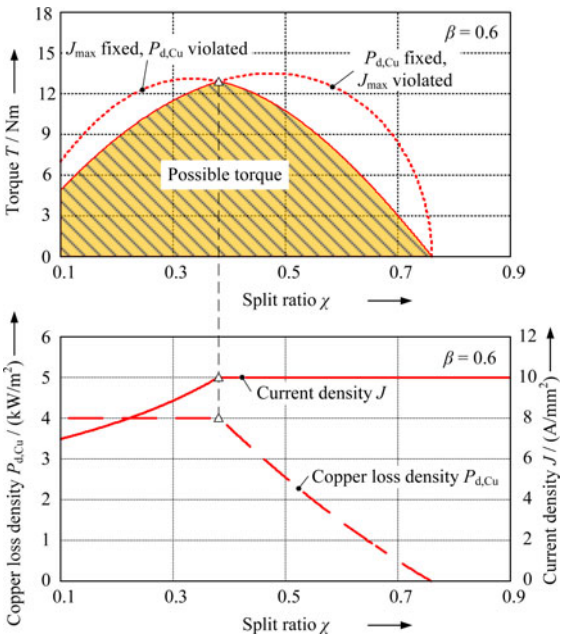

Fig. 6. Torque output for an interior rotor machine with slot number 6 is shown in the upper plot for a maximum copper loss density of 4 kW/m^2 and a maximum current density of 10 A/mm^2. The torque first follows the original curve with fixed copper losses and then changes over to the original curve with fixed current density. With this measure, both thermal conditions are fulfilled over the whole split ratio range (lower plot) ($R = 75$ mm, $l = 25$ mm, $N_{\mathrm{coil}} = 300$, and $k_{\mathrm{coil}} = 0.6$).

C. Split Ratio With Global and Local Thermal Limitation

It seems that for the chosen limitations of the copper losses and the current density, no optimal split ratio can be determined that would respect both constraints. When comparing the lower plots of Figs. 3 and 5, it can be seen that these curves are crossing the boundary at exactly the same split ratio values. For small values of the split ratio, the copper loss boundary is violated, whereas for larger values, the current density boundary is violated. In order to calculate the torque over the whole split ratio range, both (6) and (10) have to be used, which is plotted in Fig. 6. Starting with small split ratio values, (6) has to be used first with fixed maximum copper losses (see upper plot in Fig. 6). During this time, the current density is below its maximum allowed value. When increasing the split ratio, the current density in the coils becomes larger (see lower plot in Fig. 6). Once it has reached the boundary, the torque calculation has to be changed using (10). A further increase in the split ratio from that point on keeps the current density constant whereas the copper losses get reduced. Hence, both thermal conditions are fulfilled over the whole split ratio range. It can be seen in Fig. 6 that the optimal split ratio for maximum torque output is exactly where both thermal conditions have reached their maximum value. Hence, the optimal value lies between the two split ratio values according to (19) and (22).

In order to determine where to change over from one calculation to the other, the split ratio χ_{PJ} for which both thermal conditions are fulfilled at the same moment has to be calculated. This can be done by finding the intersection of (6) and (10), leading to

$$\chi_{\mathrm{PJ}} = \frac{b_{\mathrm{PJ}} - \sqrt{b_{\mathrm{PJ}}^2 - 4a_{\mathrm{PJ}}}}{2a_{\mathrm{PJ}}} \tag{25}$$

with the factors

$$a_{\mathrm{PJ}} = \frac{f_a \cdot J_{\max}^2 \cdot f_m}{J_{\max}^2 \cdot f_m - P_{\mathrm{Cu}}} \tag{26}$$

and

$$b_{\mathrm{PJ}} = \frac{2f_b \cdot J_{\max}^2 \cdot f_m}{J_{\max}^2 \cdot f_m - P_{\mathrm{Cu}}} \tag{27}$$

where f_m is a machine factor defined as

$$f_m = \rho_{\mathrm{Cu}} \cdot l \cdot k_{\mathrm{coil}} \cdot \pi \cdot R^2. \tag{28}$$

Unlike previously, several machine design parameters influence the split ratio found with (25).

IV. Choice of Optimal Split Ratio

With these calculations, it becomes apparent that the split ratio calculation highly depends on the boundary conditions for the global and local thermal values and on the motor dimensions. With (19), (22), and (25), there are three different formulas for the calculation of the optimal split ratio of a machine, leading to three different results. However, there can only be one valid solution for a certain machine setup with given thermal limitations as can be seen in Fig. 7. For four different boundary conditions for the global and local thermal limitations, the maximum possible torque is shown. It can be seen that either a reduction in the maximum copper losses (a) or an augmentation of the maximum current density (b) shifts the optimal split ratio to a higher value in comparison with Fig. 6, such that the optimal split ratio is given by (19). An augmentation of the maximum copper losses, shown in Fig. 7(c), or a reduction of the maximum current density (d), on the other hand, shifts the optimal split ratio to smaller values, wherefore the optimal split ratio is found with (22).

The validity for each of the torque and split ratio formulas has to be determined in dependence on the global and local thermal limitations. Fig. 8 illustrates the three different cases for the split ratio and torque calculation.

For all the segments 1 to 3, the copper losses are the limiting factor in the beginning for small split ratio values and (6) has to be applied. When the split ratio is further increased, the maximum current density will be reached and the transition, being the intersection of (6) and (10), to the current density based torque calculation (10) has to be done. These three sectors help to determine where this transition occurs. If the thermal constraints belong to segment 1, the intersection happens before the maximum of any of the torque curves is reached, which is the case plotted in Fig. 7(c) and (d). Hence, the torque calculation according to (10) has to be used and the optimal split ratio is found with (22). For global and local thermal limitations belonging to segment 2, the intersection happens between the two maxima of the original curves, as was treated in Fig. 6. Hence, the optimal split ratio is found using (25). The change from segment 1 to 2 occurs when the torque intersection is

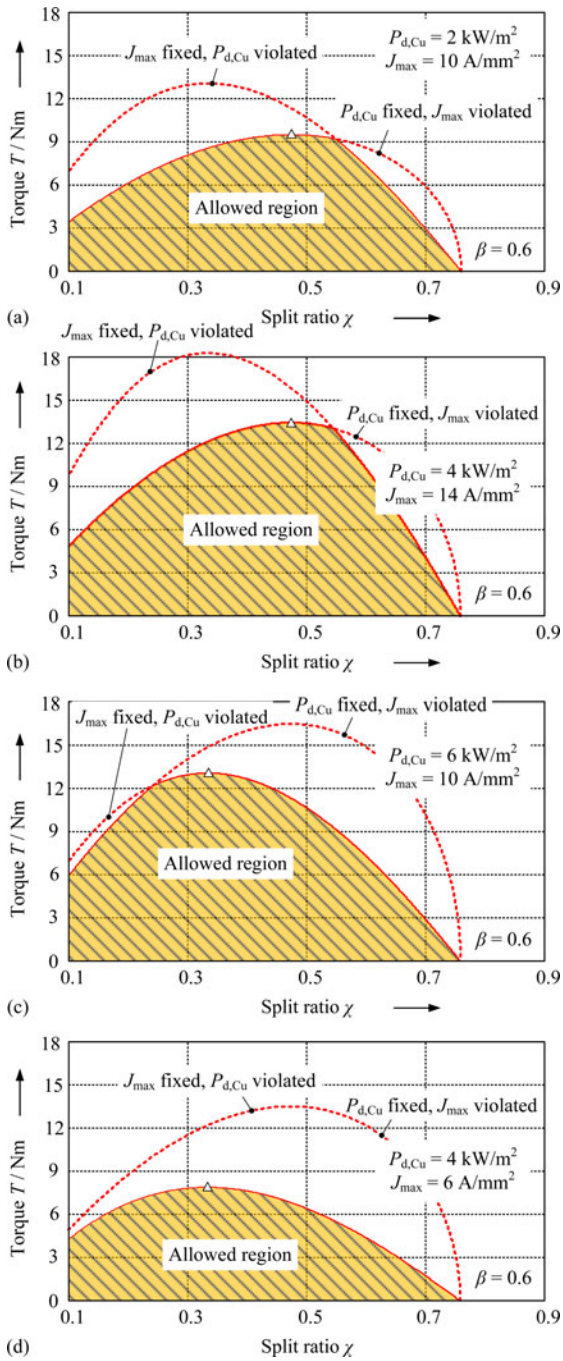

Fig. 7. Torque output for an interior rotor machine with slot number 6 is shown for a maximum copper loss density of (a) 2 kW/m^2, (b) and (d) 4 kW/m^2, and (c) 6 kW/m^2, whereas a maximum current density of (a) and (c) 10 A/mm^2, (b) 14 A/mm^2, and (d) 6 A/mm^2 has been set (R = 75 mm, l = 25 mm, $N_{\mathrm{coil}} = 300$, and $k_{\mathrm{coil}} = 0.6$).

identical with the optimal split ratio according to (22). This leads to the condition

$$P_{\mathrm{cu}} = J_{\mathrm{max}}^2 \cdot f_m \left(\frac{2f_b \cdot \sqrt{4f_b^2 - 3f_a} + 4f_b^2}{9f_a} + \frac{2}{3} \right) \quad (29)$$

for the segment change. Finally, for thermal constraints belonging to segment 3, the transition happens after the maximum of the copper loss based torque curve has been reached, which is

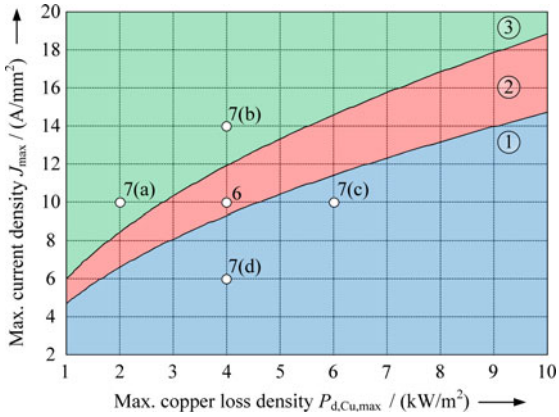

Fig. 8. Split ratio calculation is highly influenced by the choice of the maximum copper losses and the maximum current density. Three different cases can be distinguished: In segment 1, the copper losses are the limiting factor for very small values of the split ratio. But once it is increased, the maximum current density is reached and the copper losses have to be lowered. This transition happens before the maximum of the torque curve according to (10) is reached. Hence, (22) has to be applied for this first segment. In segment 2, the transition from the constraint of copper losses to the constraint of maximum current density happens in between the optimal split ratio according to (19) and (22). In this case, (25) has to be applied (see Fig. 6). Finally, in segment 3, the transition happens after the optimal split ratio according to (19) has been reached. Hence, the value of (19) has to be used. Additionally, the chosen boundary conditions used in Figs. 6 and 7(a)–(d) have been marked.

shown in Fig. 7(a) and (b). Therefore, the optimal split ratio is found with (19) and the torque maximum is calculated with (6). The change from segment 2 to 3 occurs when the torque intersection is identical with the optimal split ratio according to (19). This leads to the condition

$$P_{\mathrm{cu}} = J_{\mathrm{max}}^2 \cdot f_m \left(\frac{f_b \cdot \sqrt{9f_b^2 - 8f_a} + 3f_b^2}{8f_a} + \frac{1}{2} \right). \quad (30)$$

for the segment change.

In addition, the influence of the design (slot number and motor dimensions) on the choice of the split ratio calculation has been investigated and is presented in Fig. 9. Increasing the slot number slightly lowers the original curves from Fig. 8 (solid black lines in Fig. 9) in vertical direction, whereas the curves are slightly lifted for a slot number smaller than 6. However, this shifting of the curves is in a very small range as can be seen in Fig. 9(a).

The influence of a variation in the motor dimensions, namely, the motor radius and the motor length, are shown in Fig. 9(b) and (c), respectively. The corresponding values have been doubled first, followed by investigating the effect of dividing the corresponding parameter by factor 2. As can be seen, increasing a motor dimension lowers the curves in horizontal directions, which means that the global thermal limitation becomes more crucial. On the other hand, a decrease in a motor dimension has the opposite effect and the local thermal limitation becomes more severe. This finding can be explained with the fact that the surface through which the copper losses are dissipated only scales in a square relation, whereas the current density is linked with the motor volume resulting in a cubic relation. Therefore, it can be derived that the global thermal limitation is more crucial

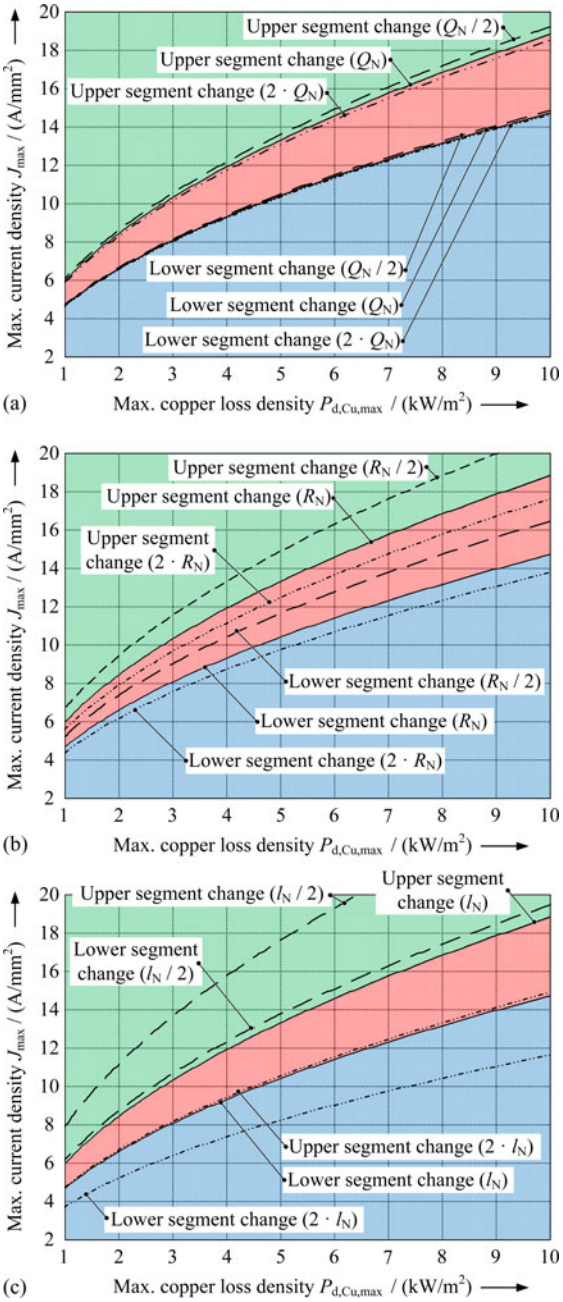

Fig. 9. Split ratio calculation is additionally influenced by the design of the motor (slot number and motor measurements). In the three plots, the black solid lines represent the original curves from Fig. 8 and the segment colors from Fig. 8 are repeated. The influence of varying the (a) slot number, (b) motor radius, and (c) motor length is investigated. In all the three cases, the value of the reference design from Fig. 8 is denoted with an index N. Then, the influence of doubling the corresponding parameter is investigated, which generally lowers the curves in vertical direction, and of dividing the parameter by factor 2, which generally lifts the curves in vertical direction.

for larger motor sizes, whereas for small motors it is the current density.

In motor theory, sometimes current sheet is used instead of current density. It links the current with the circumference of a machine, resulting in a linear scaling relation. For smaller motors, a constraint based on this current sheet can be ignored; but for larger motors, it would obviously become the dominant constraint because of the linear scaling. However, from a thermal point of view, it is a too weak criterion and should not be considered, because the relevant factor is the heat that can be dissipated through the surface. For that reason, the current sheet has not been considered for this investigation.

V. Identification of Thermal Constraints

For a practical application, the values for the maximum copper loss density and the maximum current density have to be identified first before the optimal split ratio can be calculated for a fixed machine size. The identification of these thermal limitations mainly depends on the intended cooling effort and the maximum allowed temperatures in the machine. The total copper losses are influenced by the overall motor surface. Additionally, heat sinks can be implemented in order to cope with higher losses. For the current density in the coils, on the other hand, the maximum allowed coil temperature is the influencing factor. In order to raise the maximum allowed current density, the thermal resistance from the coils to the motor surface and beyond (e.g., to the surrounding air or to a liquid) has to be lowered [14]. This can be achieved by employing a pottant with a good thermal conductivity value or by installing water cooling. For the latter, a helix built of narrow tubes needs to be placed close to the coils.

There is an interconnection between these two thermal constraints, the motor design and setup (i.e., the indented cooling effort), which is not considered in the split ratio calculation per se. Nevertheless, the optimal split ratio can be calculated as soon as the maximum allowed operating point in Fig. 8 has been identified. The analysis of this interconnection is one of the design tasks for a machine designer, as will be shown in the next section.

VI. General Design Guidelines

The model presented in this paper is intended to be used as a rough calculation tool for machine design. Following this first step, a detailed optimization based on the finite element method has to be undertaken. Nevertheless, this model gives valuable insight into where the design should aim at and already narrows down the solution space for the optimal setup in a fast way.

In Fig. 10, the curves previously derived (see Fig. 6) are compared to three dimensional finite element analysis (FEA) results. If saturation is ignored, similar values are found employing FEA, which proves the accuracy of the model. However, if saturation is considered, there is a difference between the model and the FEA for split ratio values below 0.4. This is an indicator that the iron is heavily driven into saturation. Hence, for a real setup, the optimal split ratio would rather be larger than what was predicted with the model in this paper. Yet, as mentioned earlier, it can be usefully employed for a first prediction of the achievable torque and the optimal split ratio region.

There are two important takeaway messages from this analysis. First, it was shown that there are many parameters in motor design that influence each other, namely, several machine parameters and dimensions and thermal constraints. They all have to be considered for an optimal design, which results in a very

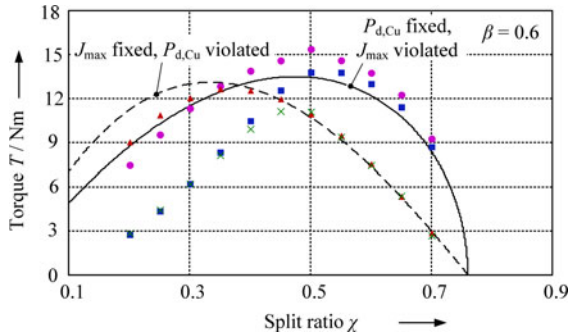

Fig. 10. Original curves from the model (copied from Fig. 6) are compared with an FEA. In the beginning, iron saturation was not considered in the FEA, resulting in the dots for fixed copper loss density and in the triangles for fixed current density.The comparison proves that the model predicts accurate values. If iron saturation is considered, however, a large difference can be found for small split ratio values below 0.4 (squares for fixed copper loss density and crosses for fixed current density). This is due to the fact that the iron is highly driven into saturation, which obviously lowers the achievable torque.

complex analysis. By following the calculation scheme provided in this paper, the complexity can be drastically reduced. This helps the motor designer to already estimate if a certain setup should be further considered or can be discarded in the first place.

Second, it is dangerous to only consider a global thermal limitation based on the motor surface. Especially, for smaller motor dimensions, local thermal limitations can become crucial. There is a risk of local overheating if the heat transfer from hot parts (coils) to the motor surface is insufficient. A motor designer has to consider the thermal design and take this risk into account. He can derive the relation between the allowed current density in the coils and the copper loss density, which then allows him evaluating the accurate torque calculation method based on the distinction from Fig. 8.

VII. Conclusion

It was shown that the optimal split ratio of a permanent-magnet interior rotor machine highly influences the achievable motor torque. There is a tradeoff for the volume distribution into iron, permanent magnet, and copper material. The latter determines the maximum achievable magnetomotive force, whereby a global and a local thermal limitation have to be respected. The global thermal limitation is related to the heat dissipation per motor surface, whereas the local limitation addresses the current density directly in the coils. Both limitations are influenced by aspects of the motor design and setup, such as the thermal resistance of the motor materials and the installation of additional heat sinks. Once the thermal limitations are identified, a conclusion can be drawn on the influence of each limitation and, finally, the optimal split ratio and the maximum achievable torque can be determined.

References

[1] A. M. El-Refaie, "Fractional-slot concentrated-windings synchronous permanent magnet machines: opportunities and challenges," *IEEE Trans. Ind. Electron.*, vol. 57, no. 1, pp. 107–121, Jan. 2010.

[2] M. Barcaro, N. Bianchi, and F. Magnussen, "Remarks on torque estimation accuracy in fractional-slot permanent-magnet motors," *IEEE Trans. Ind. Electron.*, vol. 59, no. 6, pp. 2565–2572, Jun. 2012.

[3] M. Pinilla and S. Martinez, "Selection of main design variables for low-speed permanent magnet machines devoted to renewable energy conversion," *IEEE Trans. Energy Convers.*, vol. 26, no. 3, pp. 940–945, Sep. 2011.

[4] L. Jian, G. Xu, C. C. Mi, K. T. Chau, and C. C. Chan, "Analytical method for magnetic field calculation in a low-speed permanent-magnet harmonic machine," *IEEE Trans. Energy Convers.*, vol. 26, no. 1, pp. 862–870, Mar. 2011.

[5] J. A. Güemes, A. M. Iralagoitia, J. I. Del Hoyo, and P. Fernández, "Torque analysis in permanent-magnet synchronous motors: A comparative study," *IEEE Trans. Energy Convers.*, vol. 26, no. 1, pp. 55–63, Mar. 2011.

[6] M. Galea, C. Gerada, T. Raminosoa, and P. Wheeler, "A thermal improvement technique for the phase windings of electrical machines," *IEEE Trans. Ind. Appl.*, vol. 48, no. 1, pp. 79–87, Jan./Feb. 2012.

[7] R. Wrobel, P. H. Mellor, and D. Holliday, "Thermal modelling of a segmented stator winding design," *IEEE Trans. Ind. Appl.*, vol. 47, no. 5, pp. 2023–2030, Sep./Oct. 2011.

[8] Z. Kolondzovski, A. Arkkio, J. Larjola, and P. Sallinen, "Power limits of high-speed permanent-magnet electrical machines for compressor applications," *IEEE Trans. Energy Convers.*, vol. 26, no. 1, pp. 73–82, Mar. 2011.

[9] A. Boglietti, A. Cavagnino, and D. A. Staton, "Determination of critical parameters in electrical machine thermal models," *IEEE Trans. Ind. Appl.*, vol. 44, no. 4, pp. 1150–1159, Jul./Aug. 2008.

[10] F. B. Chaaban, "Determination of the optimum rotor/stator diameter ratio of permanent magnet machines," *Elect. Mach. Power Syst.*, vol. 22, no. 4, pp. 521–531, 1994.

[11] Y. Pang, Z. Q. Zhu, and D. Howe, "Analytical determination of optimal split ratio for permanent magnet brushless motors," in *IEE Proc. Elect. Power Appl.*, vol. 153, no. 1, pp. 7–13, Feb. 2006.

[12] L. J. Wu, Z. Q. Zhu, J. T. Chen, Z. P. Xia, and G. W. Jewell, "Optimal split ratio in fractional-slot interior permanent-magnet machines with non-overlapping windings," *IEEE Trans. Magn.*, vol. 46, no. 5, pp. 1235–1242, May 2010.

[13] Y. Shen and Z. Q. Zhu, "Analytical prediction of optimal split ratio for fractional-slot external rotor PM brushless machines," *IEEE Trans. Magn.*, vol. 47, no. 10, pp. 4187–4190, Oct. 2011.

[14] D. A. Stator and A. Cabagnino, "Convection heat transfer and flow calculations suitable for electric machines thermal models," *IEEE Trans. Ind. Electron.*, vol. 55, no. 10, pp. 3509–3516, Oct. 2008.

Thomas Reichert (S'09–M'13) was born in Schaffhausen, Switzerland, in 1983. He received the M.Sc. degree in electrical engineering and information technology from the Swiss Federal Institute of Technology (ETH) Zurich, Zurich, Switzerland, in 2008, and the Ph.D. degree (high-torque and high-speed magnetically levitated motors) from the Power Electronic Systems (PES) Laboratory, Swiss Federal Institute of Technology Zurich, in 2013.

During his studies, he was involved in mechatronics, robotics, power systems, and control. During his master's thesis, he simulated rotor dynamics and implemented a magnetic bearing for a mega-speed drive.

Thomas Nussbaumer (S'02–M'06) was born in Vienna, Austria, in 1975. He received the M.Sc. degree (with Hons.) in electrical engineering from the University of Technology Vienna, Vienna, in 2001, and the Ph.D. degree from the Power Electronic Systems (PES) Laboratory, Swiss Federal Institute of Technology (ETH) Zurich, Zurich, Switzerland, in 2004.

From 2001 to 2006, he was with PES, where he was involved in research on modeling, design, and control of three-phase rectifiers, power factor correction techniques, and electromagnetic compatibility. Since 2006, he has been with Levitronix GmbH, Zurich, Switzerland, where he is involved in bearingless motors, magnetic levitation, and permanent-magnet motor drives for the semiconductor and biotechnology industry. His current research interests include compact and high-performance mechatronic systems, including novel power electronics topologies, control techniques, drive systems, sensor technologies, electromagnetic interference (EMI), and thermal aspects.

Johann W. Kolar (F'10) received the M.Sc. and Ph.D. degrees (*summa cum laude/promotio sub auspiciis praesidentis rei publicae*) from the University of Technology Vienna, Vienna, Austria.

Since 1984, he has been an Independent International Consultant in close collaboration with the University of Technology Vienna, in the fields of power electronics, industrial electronics, and high performance drives. He has proposed numerous novel converter topologies and modulation/control concepts, e.g., the VIENNA Rectifier, the Swiss Rectifier, and the three-phase AC–AC Sparse Matrix Converter. He has authored or coauthored more than 450 scientific papers in international journals and conference proceedings and has filed more than 85 patents. In 2001, he was appointed Professor and Head of the Power Electronic Systems Laboratory, Swiss Federal Institute of Technology (ETH) Zurich, Zurich, Switzerland. His current research interests include AC–AC and AC–DC converter topologies with low effects on the mains, e.g., for data centers, More-Electric-Aircraft and distributed renewable energy systems, Solid-State Transformers for Smart Microgrid Systems, realization of ultra-compact and ultra-efficient converter modules employing latest power semiconductor technology (SiC and GaN), micropower electronics and/or Power Supplies on Chip, multidomain/scale modeling/simulation and multiobjective optimization, physical model-based lifetime prediction, pulsed power, and ultrahigh speed and bearingless motors.

Dr. Kolar received the Best Transactions Paper Award of the IEEE Industrial Electronics Society in 2005, the Best Paper Award of the ICPE in 2007, the First Prize Paper Award of the IEEE Industry Applications Society (IAS) Industrial Power Converter Committee (IPCC) in 2008, the IEEE Annual Conference of the IEEE Industrial Electronics Society (IECON) Best Paper Award of the IES PETC in 2009, the IEEE Power Electronics Society (PELS) Transaction Prize Paper Award 2009, the Best Paper Award of the IEEE/ASME Transactions on Mechatronics 2010, the IEEE PELS Transactions Prize Paper Award 2010, the Best Paper First Prize Award at the Energy Conversion Congress & Exhibition (ECCE) Asia 2011, and the First Place IEEE IAS Society Prize Paper Award 2011. Furthermore, he received the ETH Zurich Golden Owl Award 2011 for excellent teaching. He also received an Erskine Fellowship from the University of Canterbury, New Zealand, in 2003. He initiated and/or is the founder/cofounder of four spin-off companies targeting ultrahigh speed drives, multidomain/level simulation, ultra-compact/efficient converter systems, and pulsed power/electronic energy processing. In 2006, the European Power Supplies Manufacturers Association (EPSMA) awarded the Power Electronics Systems Laboratory of ETH Zurich as the leading academic research institution in Power Electronics in Europe. He is a Member of the IEEJ and the International Steering Committees and Technical Program Committees of numerous international conferences in the field (e.g., Director of the Power Quality Branch of the International Conference on Power Conversion and Intelligent Motion). He is the founding Chairman of the IEEE PELS Austria and Switzerland Chapter and the Chairman of the Education Chapter of the EPE Association. From 1997 through 2000, he was an Associate Editor of the IEEE TRANSACTIONS ON INDUSTRIAL ELECTRONICS. Since 2001, he has been an Associate Editor of the IEEE TRANSACTIONS ON POWER ELECTRONICS. Since 2002, he has been an Associate Editor of the *Journal of Power Electronics* of the Korean Institute of Power Electronics and a Member of the Editorial Advisory Board of the *IEEJ Transactions on Electrical and Electronic Engineering*.